Design and fabrication of a dual-polarized, dual-band reflectarray using optimal phase distribution

Iman ARYANIAN[1,*], Arash AHMADI[2], Mehdi RABBANI[1], Sina HASSIBI[1],
Majid KARIMIPOUR[1]

[1]Iran Telecommunication Research Center, Tehran, Iran
[2]Department of Electrical Engineering, K. N. Toosi University of Technology, Tehran, Iran

Abstract: Two main factors limiting the reflectarray bandwidth are different phase slopes versus the frequency at every point on the aperture and the phase limitation of comprising elements at different frequencies. Considering these two factors, a novel design method is proposed to implement a dual-band, dual-polarized reflectarray antenna in X and Ku bands. An optimization algorithm is adopted to find the optimum phase for each unit cell on the reflectarray aperture. The best geometrical parameters of the phasing elements are suggested based on the phase variation of the element versus frequency and the element position with respect to the antenna feed. Many different classes of phasing elements with identical base structures are investigated to provide a lookup table for the optimization algorithm. The optimum phases are obtained so that two collimated beams are realized within the frequencies of 10.95 GHz to 11.7 GHz and 14 GHz to 14.5 GHz with vertical and horizontal polarizations, respectively. From the experimental results, the peak directivity of 27.1 dBi and 30.6 dBi, aperture efficiency of 42% and 67%, and cross-polarization level of less than –15 dB and –20 dB were obtained in the lower and upper bands, respectively.

Key words: Dual-band, dual-polarized antenna, reflectarray, optimization

1. Introduction

Reflectarray (RA) structures consist of flat platforms of phasing elements, which are arranged in a regular or irregular lattice. These elements reradiate the impinging plane wave from a space feeder as a wave with a specific phase front. These antennas benefit from known advantages of array antennas and conventional solid reflector antennas [1]. Apart from conventional reflector antennas, the aperture field distribution on the reflecting surface of an RA can be engineered only by tailoring the phasing elements. This leads to developing broadband, multiband, dual, and circular polarized RAs or advanced passive and active RA configurations with beam shaping, beam scanning, nonlinear, and beam switching capabilities, which are well suited for several applications [1–10]. In advanced designs, the reflector platform can be incorporated with horn array antennas and develop a high gain multifunction structure, which is feasible only by adjusting the phase response of the unit cells for each horn antenna [11]. As a factor of superiority compared to the phase array antennas, reflectarrays use the free space as a transmission medium between the feed and phasing elements and undoubtedly mitigate the feeding loss. Reflectarrays suffer from narrow bandwidth, which is a consequence of the bandwidth limitation of phasing elements and differential spatial phase delays. Different path lengths between the feed and each point

---

*Correspondence: aryanian@itrc.ac.ir

on the wave front of the radiated beam result in spatial phase delays [1]. Developing a reflectarray with dual closely separated frequency bands and orthogonal polarizations has become a research interest in recent years. This kind of reflectarray fulfills the requirements of a transceiver of the ground terminal for Direct Broadcast Satellite (DBS) applications [6, 8]. Merging two independent functionalities in one structure reduces the antenna space occupation without sacrificing the antenna performance. Many efforts have been made in recent years to realize dual band and/or dual-orthogonal polarization reflectarrays with acceptable performance [9, 12–16]. The main challenge in these configurations is the realization of unit cells with independent reflective phase for both bands and high copolarization isolation. For example, the authors in [17] employed the combination of double split cross loops for horizontal polarization and double split square loops for vertical polarization over the same substrate. These structures operate nearly independent in the two bands.

In [18], a comprehensive investigation was done of the reflectarray bandwidth issue. For brevity, it can be inferred that the phase compensation versus frequency is a strict function of F/D and the local position of the cell on the reflectarray aperture from the feed point of view, where F and D are the focal length and aperture size of the antenna, respectively. This factor along with the frequency dispersion at extreme frequencies of the band, which is due to bandwidth limitation of the element, are the main reasons for the narrowband behavior of a reflectarray. From the above considerations, it becomes apparent that in order to achieve an increased operational bandwidth, two solutions may be followed. First, the applied elements should have enough reflection phase ranges across the band of interest. Second, the reflection phase slope versus the frequency should follow the ideal phase slope defined in [18]. This scenario becomes more prominent for implementing dual band or multiband reflectarrays. Considering that the ideal reflection phase slope for each unit cell is dependent on the unit cell position in the aperture, the individual elements on the RA aperture must have different phase slopes in terms of frequency. Since an ordinary element is unable to provide all the required phase ranges, a common behavior over frequency, and all the required phase slopes simultaneously, the bandwidth will be reduced, especially in large reflectarrays. That is why in large RAs the difference between the phase slopes at each position on the aperture is more than in small structures [18].

In this paper, we intend to develop a dual-band linear orthogonal polarization reflectarray with enhanced bandwidth by addressing the aforementioned bandwidth limiting factors. In order to mitigate the phase error discussed above within the two frequency bands, two steps including tabulation process and searching algorithm are adopted. In the preliminary step, a lookup table is provided from reflection phases of the element by full-wave simulation tools. Doing so, a parametric study is accomplished over different classes of phasing elements by considering two separate polarizations for the impinging wave. Second, an appropriate search algorithm is performed on the full-wave simulation results to get the best geometrical parameters for the elements according to the required phase responses. This algorithm operates according to two criteria: the element positions with respect to the feed, which forces the required phase slope for that position, and the phase range of the element as the frequency is varied. These two factors minimize the overall phase error within both bands. The element in the design process is the modified one reported in [17] to achieves more bandwidth, specifically in the upper band.

2. Unit cell design and simulation

Figure 1a shows the proposed unit cell configuration along with its geometrical parameters. The unit cell is composed of interlaced metal patches etched on the same substrate. The position of the patch of both bands relative to each other is selected for realizing dual polarization operation. The applied element enables

the designer to control the reflecting phase for both bands independently and with small magnitude loss. Investigations showed that for all states of the unit cell dimensions in both bands, the losses are less than 0.1 dB, leading to negligible degradation in antenna performance and especially radiation efficiency. As can be shown in Figure 1b, a gap with a given width, which has a capacitive feature, is generated on the metal patch for both bands to convert the element from the polarization-insensitive element to the polarization-sensing one. Notably, low frequency-sensitive behavior, acceptable phase swing range, and a gentle phase variation with respect to the patch length, which results in relaxing the fabrication tolerances for both bands, are the main reasons for choosing this element. All of the geometrical parameters and their values for generating a suitable database of phase responses are presented in the captions of Figures 1a and 1b.

(a)   (b)
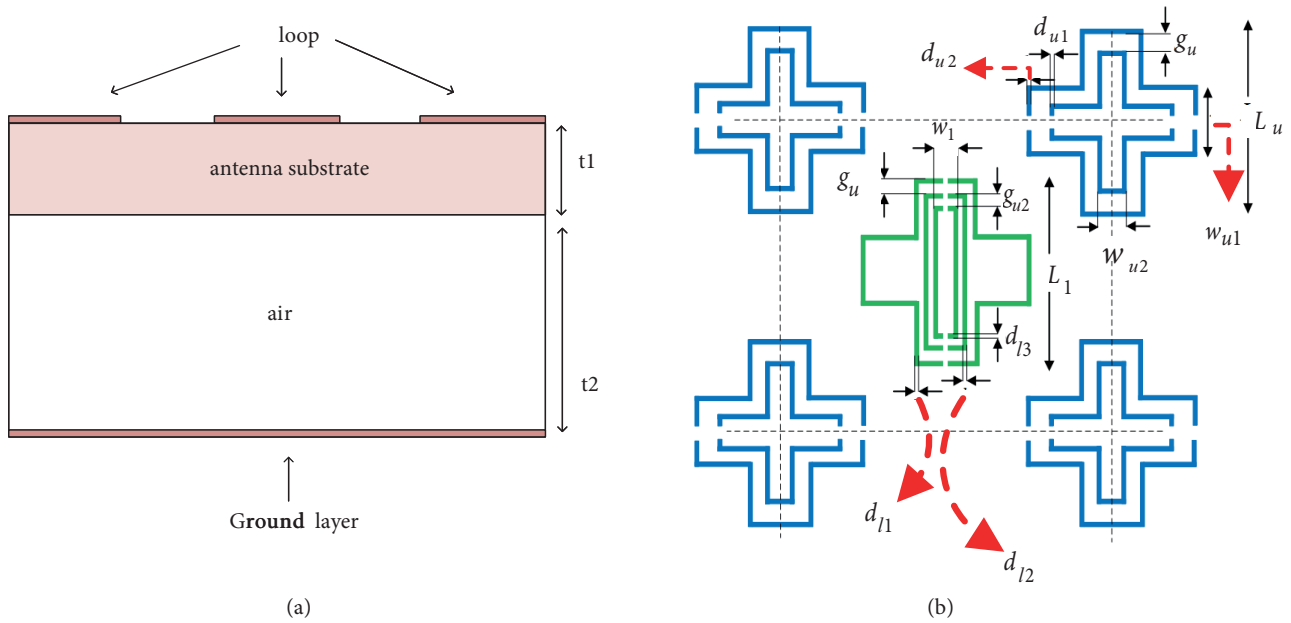
Figure 1. Demonstration of the proposed unit cell along with its geometrical parameters. (a) Side view. (b) Top view. Lookup table is provided by parametric study of the element as follows: dl1 = dl2 = dl3 = 0.2 mm : 0.1 mm : 0.5 mm, gu1 = gu2 = 0.2 mm : 0.1 mm: 0.6 mm, w1 = 2.5 mm, L1 = 5.5 : 0.2 mm : 10.1 mm, du1 = du2 = 0.2 mm, gu = 0.6 mm, Wu1 = 1 mm : 0.5 mm : 3.5 mm, Wu2 = 0.6 mm: 0.5 mm : 3.1 mm, Lu = 3.5 mm : 0.2 mm : 8 mm. Cell size is 14 mm. The substrate is RT5880 with $\varepsilon_r = 2.2$. Parameters t1 and t2 are t1 = 1.57 mm, t2 = 3 mm.

All full-wave simulations are performed by HFSS, placing the element in a periodic boundary condition in the x and y directions and using Floquet modes in the z direction. Figure 2 show two samples of the phase responses of an element versus the patch lengths (L1 is swept in the lower band and Lu is swept in the upper band). Other geometrical parameters of the element are given in the caption of Figure 2. Clearly, the phase response covers a wide range beyond a cycle of 360° with a gentle slope versus the patch length. In addition, it is observed that the element has similar behavior at the center and extreme frequencies in both bands.

The interlaced arrangement of metal patches in single layer configurations suffers from the mutual coupling issues between the elements of both bands. This factor should be investigated especially for the case where the minimum separation between the two elements occurs. Figures 3a–3f show several possible reflection phases that correspond to various patch lengths in the two bands. Other geometrical parameters, which are defined in Figure 2b, remain unchanged. Clearly, we can obtain other reflection phase distributions by sweeping other geometrical parameters in the two bands. As shown in Figures 3a–3f, the effect of patch length variations in the
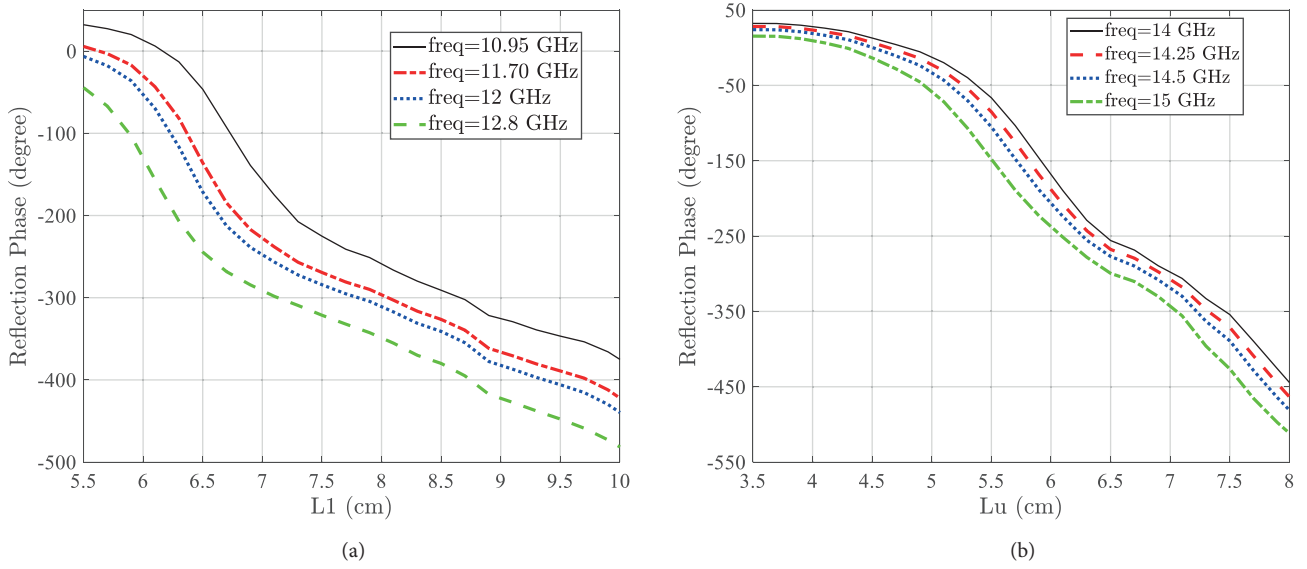
Figure 2. Simulated results of reflection phase at different frequencies. (a) Reflection phases in the lower band for Lu = 8 mm. (b) Reflection phases in the upper band for L1 = 5 mm. Other parameters are identical for both curves as dl1 = dl2 = dl3 = 0.3, gu1 = gu2 = 0.3 mm, du1 = du2 = 0.2 mm, gu = 0.6 mm, wu1 = 4 mm, wu2 = 2 mm.

lower band on the element in the upper band and vice versa is negligible except for L1 > 9 mm. For large values of L1, the element of the lower band has a destructive effect on the upper band's phase response. Alternatively, these lengths (L1> 9 mm) can be omitted from the search space in the optimization process. It is worthwhile to point out that the copolarization amplitude of the reflected wave is higher than 0.98 and the cross-polarization amplitude is lower than 0.05 in both bands. This causes a decrease of the cross-polarization level of the antenna in the two bands. In the second step, we proceed to find the optimal geometrical parameters of the element based on two criteria: the element location on the antenna aperture and the element phase response at center and extreme frequency bands. Doing so, the error function given in Eq. (1) is defined, which must be minimized to accelerate the search for the best element routine.

$$e(m,n) = \sum_{i=c_1,l_1,u_1} \left| \Phi^{desired}_{f_i,\theta_{mn},\varphi_{mn}}(m,n) - \Phi^{achieved}_{f_i,\theta_{mn},\varphi_{mn}}(m,n) \right| + \sum_{i=c_2,l_2,u_2} \left| \Phi^{desired}_{f_i,\theta_{mn},\varphi_{mn}}(m,n) - \Phi^{achieved}_{f_i,\theta_{mn},\varphi_{mn}}(m,n) \right|.$$

(1)

The error function defined in Eq. (1) is the modified version of the functions presented in [19], in which the element position is introduced as a determinative factor according to [18]. The quantity desired, $\Phi^{desired}_{f_i,\theta_{mn},\varphi_{mn}}$, is the desired phase that must be satisfied by the radiation elements at the three frequencies of f_l, f_u, and f_c. Similarly, the quantity $\Phi^{achieved}_{f_i,\theta_{mn},\varphi_{mn}}$ is the realizable phase by the physical elements. The parameters θ_{mn} and φ_{mn} are the polar angles from the feed point of view, which determine the element position on the aperture. The parameters c_1, l_1, and u_1 are assigned to the center, lower, and higher frequencies of the lower band and the parameters c_2, l_2, and u_2 are dedicated to the upper band. Note that the error function defined in Eq. (1) guarantees that different phase behaviors of the element at any location of the reflective surface will be accounted for in the design process. To show the adverse behavior of frequency factor on the reflective phase of the elements at various points of the aperture, the desired phase slope versus the frequency is calculated according to the following equation [15]:
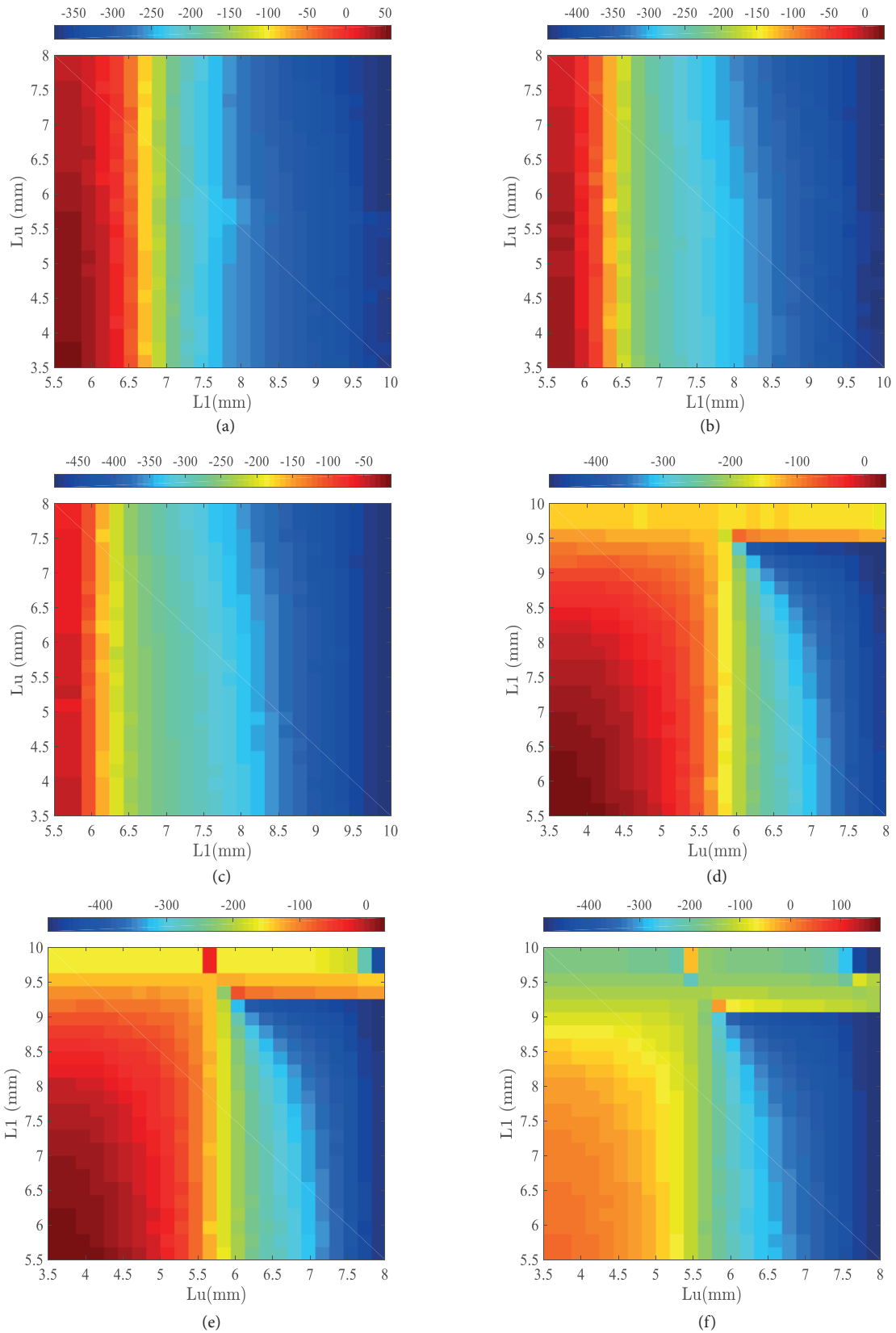
Figure 3. The 2-D demonstration of reflection phases versus length L1 and Lu for both bands. (a) f = 10.95 GHz, (b) f = 12 GHz, (c) f = 12.8 GHz, (d) f = 14 GHz, (e) f = 14.25, (f) f = 14.5 GHz.

$$\Phi(x, y, f) = -2\pi \frac{f}{c} \left[F \left(\sqrt{1 + \frac{0.5}{(F/D)^2}} - 1 \right) - \left(\sqrt{F^2 + x^2 + y^2} - F \right) \right], \qquad (2)$$

where F and D are the focal point and aperture diameter, respectively. Figure 4a depicts the desired reflection phase variation as the frequency is changed from 10 GHz to 15 GHz. The parameters D and F are considered to
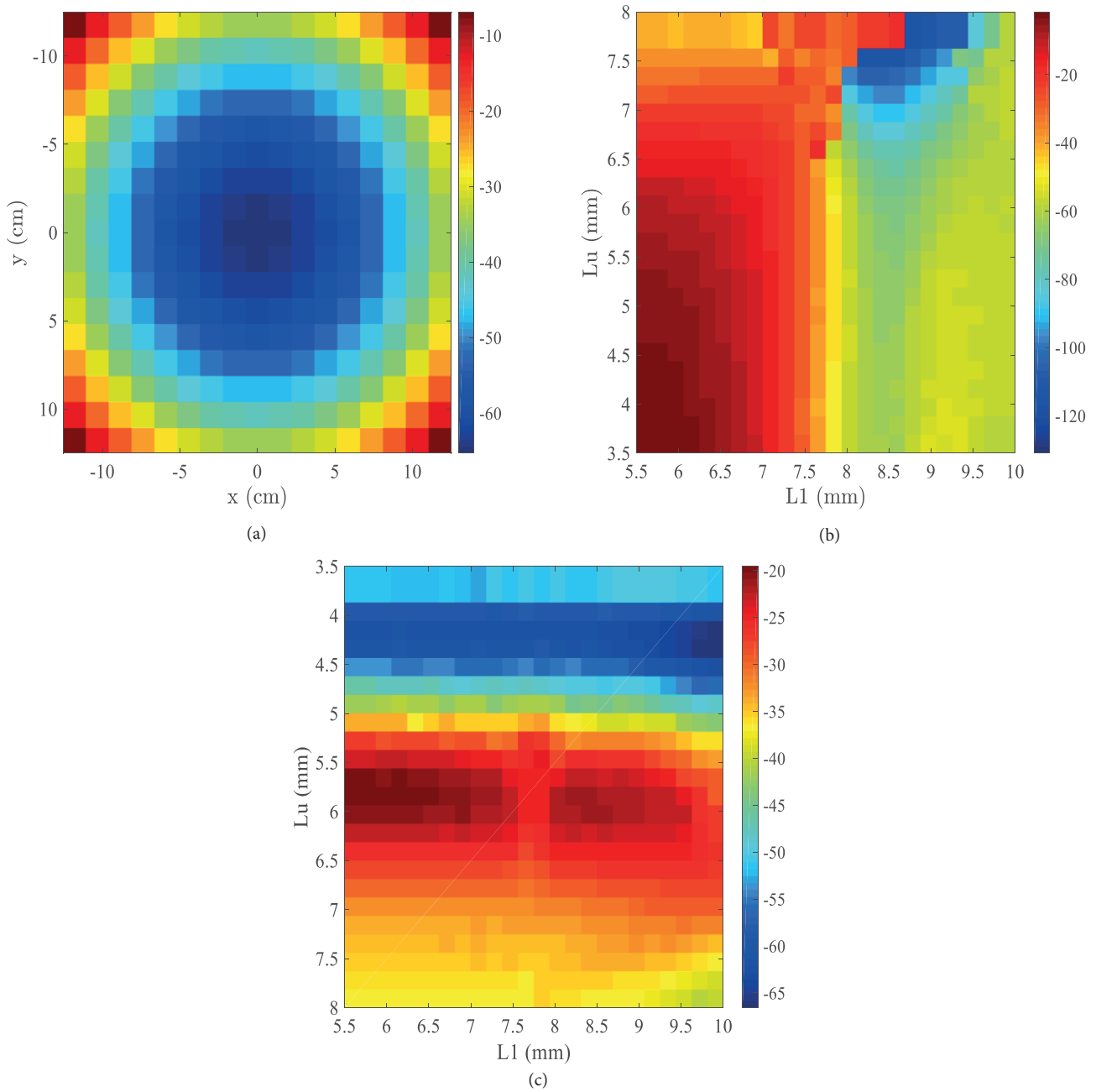
Figure 4. 2-D demonstration of reflection phase slope versus frequency for every point on the aperture. (a) Required phase slopes from 10 GHz to 15 GHz according to Eq. (2). (b, c) Realizable phase slopes of the proposed element in the upper and lower bands, respectively, by only varying L1 and Lu parameters. Other parameters remain fixed as represented in Figure 2. All phase slopes are represented in degree/GHz.

be 25 cm and 15 cm, respectively. The unit cell dimension is 14 mm $\times$ 14 mm. Figures 4b and 4c demonstrate the realizable phase slopes of the proposed element in the upper and lower bands, respectively, by only varying L1 and Lu. Simulation results show that the element has the potential to follow the variation of the required phases at each location on the aperture. The desired phase presented in Eq. (1) for each frequency in the two bands is obtained from the following well-known equation:

$$\psi_{mn} = k_0 \left[R_{mn} - (x_{mn} \cos \varphi_b + y_{mn} \sin \varphi_b) \sin \theta_b \right]. \tag{3}$$

This phase is needed to convert the spherical wave phase front to a plane wave in the (θ_b, φ_b) direction. In Eq. (3), k_0 is the free space wave number, R_{mn} is the spatial distance between the feed antenna and the mnth element, and (x_{mn}, y_{mn}) shows the coordinates of each cell.

3. Antenna design

In order to benchmark the usefulness of the proposed design method, a 25 cm $\times$ 25 cm reflectarray composed of 324 elements described in Section 2 has been designed to operate in the X and Ku bands with center frequencies of 11.3 GHz and 14.25 GHz. The desired beam directions for both bands is considered $(\theta, \varphi) = (0°, 10°)$. The searching process to find the best geometrical parameters for the elements was done by considering $f_L = 10.95\,GHz$ & $14\,GHz$ and $f_H = 11.7 GHz$ & $14.5\,GHz$ as extreme frequencies of the lower and upper band, respectively. After implementing the optimization method, the optimal geometrical parameters of the elements for both bands have been obtained. The final optimal arrangement of the elements of the antenna is depicted in Figure 5. Two pyramidal horn antennas with a q factor of 2.5 and 3 were employed as the reflectarray feeder for the X and the Ku bands, respectively. Considering these q factors, the two focal lengths are calculated to be 15 cm and 20 cm for the lower and upper frequency bands, respectively. These focal lengths achieve the maximum aperture efficiency [20]. Two feeds are aligned to the aperture with an offset of 30° around the x axis. A prototype of the antenna was manufactured (see Figure 6).
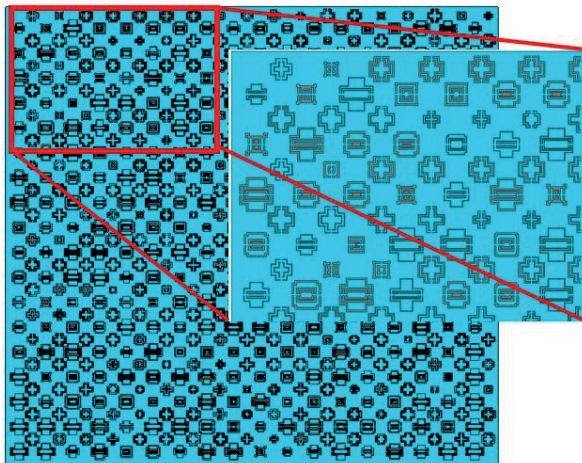

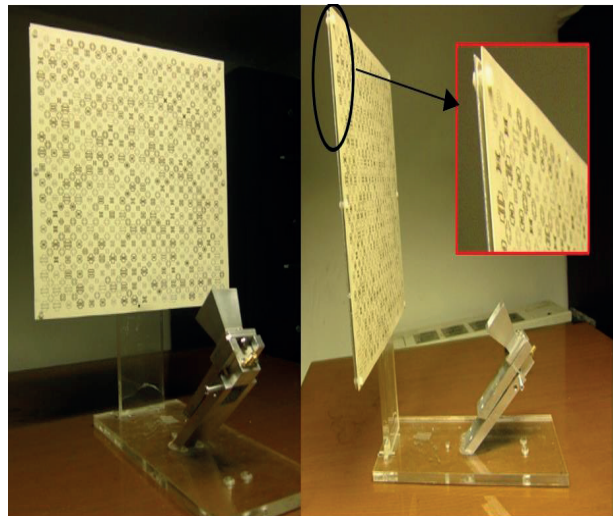**Figure 5**. Arrangement of the elements with the optimized dimensions.

Figure 6. The prototype of the proposed antenna.

The far-field patterns were measured in an anechoic chamber. The comparisons between the simulation and experimental results of the antenna are depicted in Figures 7a–7c for the lower band and Figures 8a–8c for

the upper band. These plots show good agreement between the numerical and experimental results. Side lobe levels below –10 dB and –13 dB and cross-polarization levels below –15 dB and –20 dB were obtained for the lower and upper bands, respectively. The 3-dB beam width of the antenna for the frequencies of 10.9 GHz, 11.3 GHz, and 11.7 GHz are 5.54, 5.37, and 5.18 degrees, respectively. Similarly, 3-dB beam width quantities for the frequencies of 14 GHz, 14.25 GHz, and 14.5 GHz are 4.7, 4.3, and 4.9 degrees, respectively. Some discrepancies between the simulations and measurements are eventually due to the fabrication errors. The maximum aperture efficiencies are achieved at 10.95 GHz and 14.25 and are equal to 45% and 67%, respectively. Experimental results of the peak gains for both bands are presented in Figures 9a and 9b. It is clear that the element arrangements obtained from the search algorithm have led to acceptable bandwidth within the predefined bands.
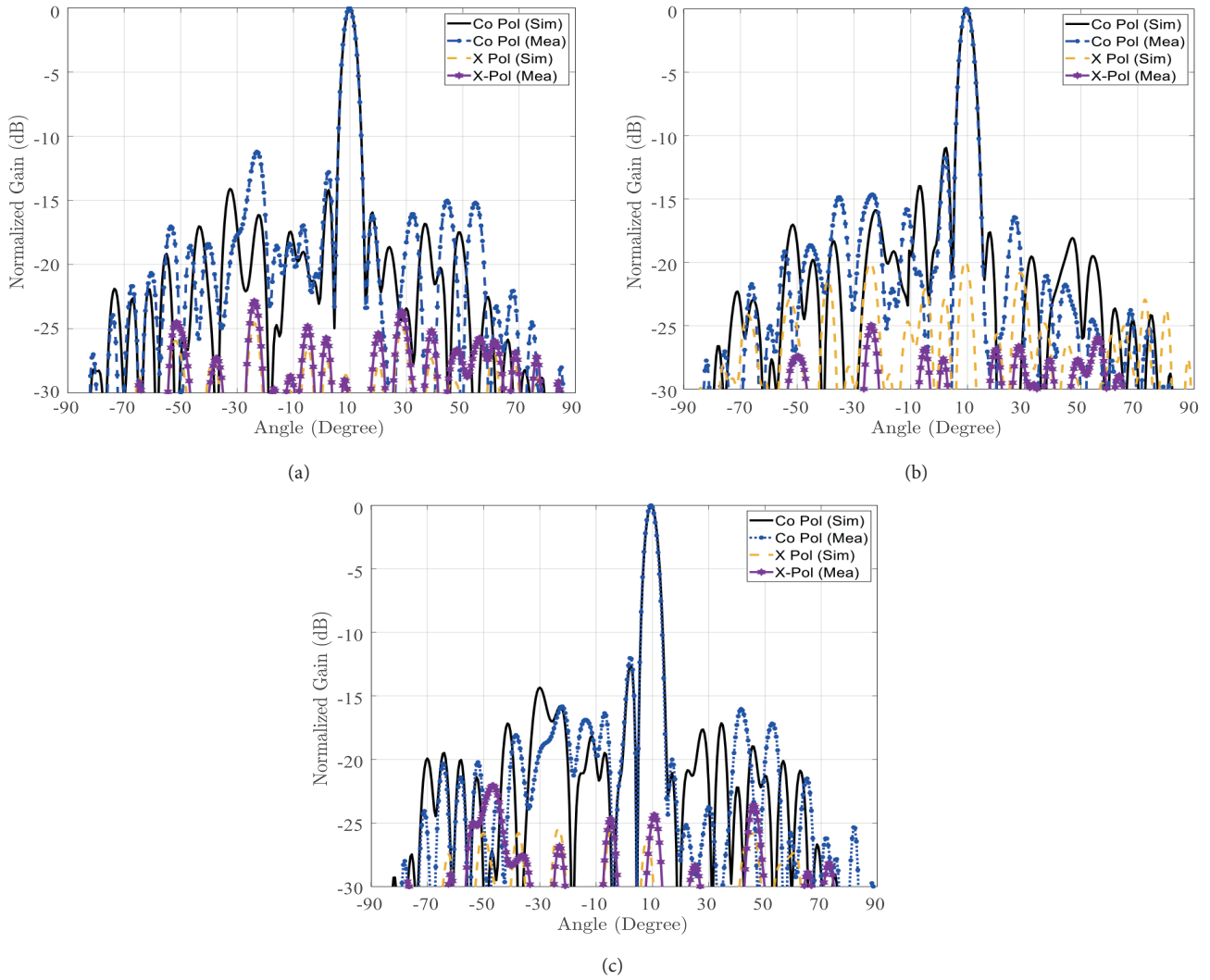

(a)

(b)

(c)
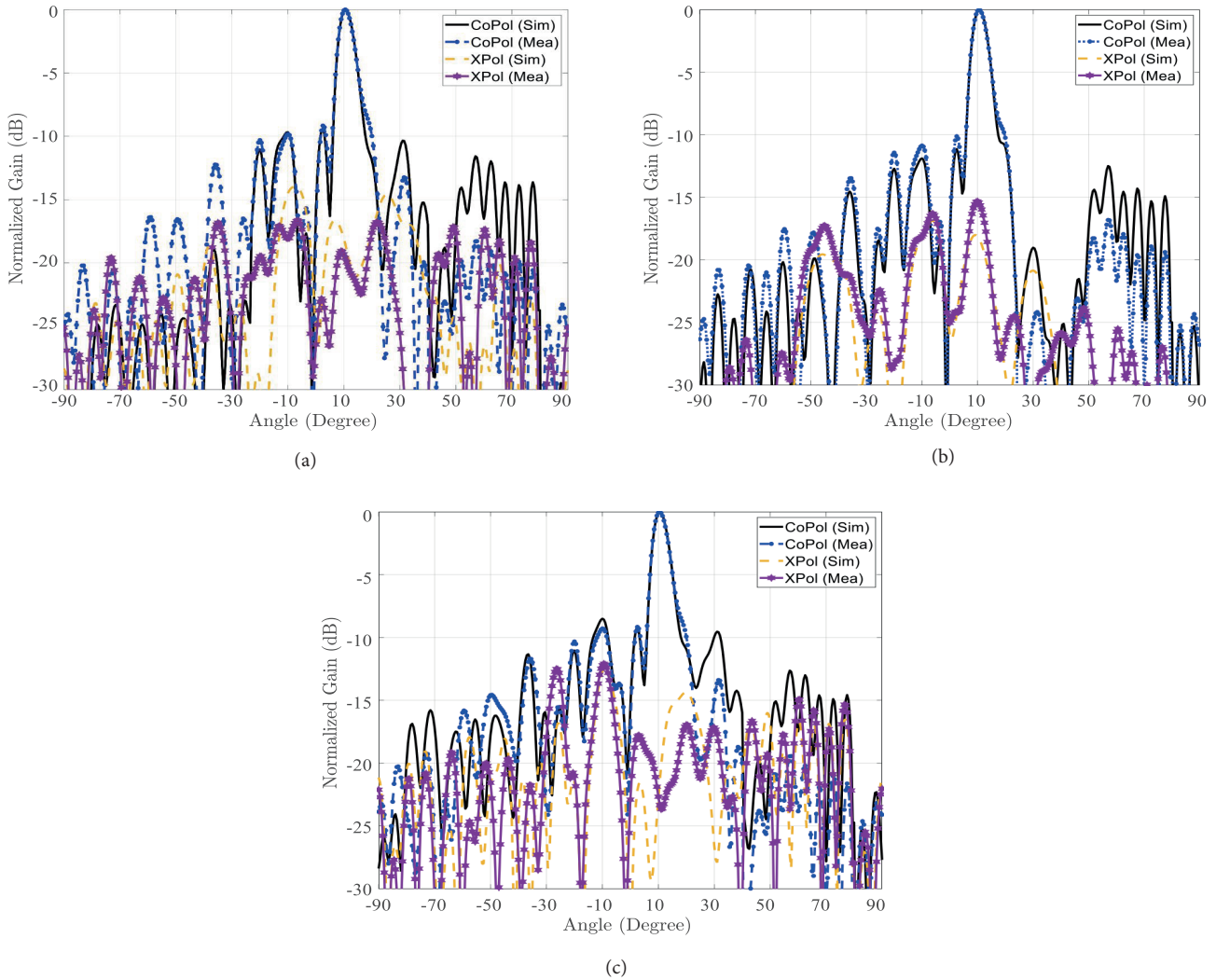
Figure 7. Simulation and measurement results of the far field gains for the lower bands at (a) 10.90 GHz, (b) 11.30 GHz, (c) 11.70 GHz.
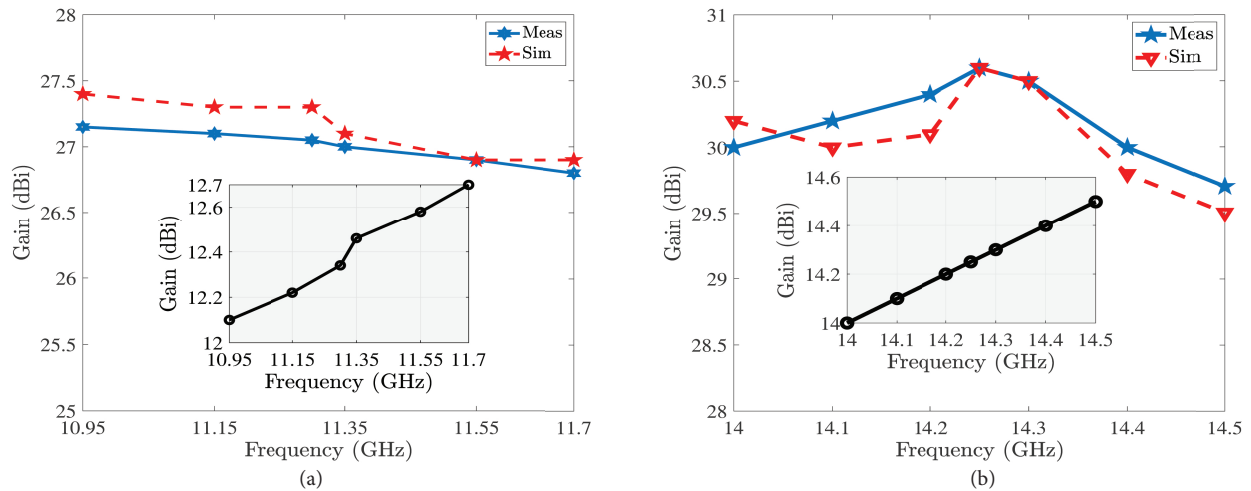
4. Conclusion

An optimized method to design a dual-band dual-polarized reflectarray with increased bandwidth has been introduced in this paper. The method was developed based on element behavior at different frequencies and

Figure 8. Normalized simulation and measurement results of the far field patterns for the upper bands: (a) f = 14 GHz, (b) f = 14.25 GHz, (c) f = 14.5 GHz.

Figure 9. The simulation and experimental results of the peak gain values versus frequency for the proposed reflectarray: (a) lower band, (b) upper band.

886

considering the element positions on the aperture. The latter determines the desired phase slope of the reflection coefficient of the element versus the frequency. A polarization-sensitive unit cell with interlaced configuration leading to several degrees of freedom in the two bands has been developed to meet our expectations. The antenna was designed to work in two frequency bands of 10.95 GHz to 11.7 GHz and 14 GHz to 14.5 GHz. In the two bands, the antenna polarizations are orthogonal to each other. Measurement results show that the maximum directivities of the antennas are 27.1 dB and 30.6 dB in the lower and upper bands, respectively. The cross-polarization levels of the antenna are –15 dB and –20 dB in the lower and upper frequency bands, respectively.

References

[1] Shaker J, Chaharmir MR, Ethier J. Reflectarray Antennas: Analysis, Design, Fabrication, and Measurement. Boston, MA, USA: Artech House, 2014.

[2] Karimipour M, Komjani N. Bandwidth enhancement of electrically large shaped-beam reflectarray by modifying the shape and phase distribution of reflective surface. Int J Electron Commun 2016; 5: 530-538.

[3] Karimipour M, Pirhadi A, Ebrahimi N. Accurate method for synthesis of shaped-beam non-uniform reflectarray antenna. IET Microwave Antennas Propag 2013; 5: 1247-1253.

[4] Karimipour M, Komjani N, Abdolali A, Abbaszade A. Optimum design of dual band shaped-beam circularly polarized reflectarray antenna based on physical optic method. Int J RF Microwave Comput-Aided Eng 2016; 8: 690-702.

[5] Aryanian I, Abdipour A, Moradi G. Studying the nonlinear performance of an amplifying reflectarray antenna. Int J Microw Wirel Technol 2017; 9: 481-491.

[6] Aryanian I, Abdipour A, Moradi G. Nonlinear analysis of active aperture coupled reflectarray antenna containing varactor diode. Appl Comput Electromagn Soc J 2015; 30: 1102-1108.

[7] Aryanian I, Abdipour A, Moradi G. Design fabrication and test of an X-band dual polarized aperture coupled reflectarray element for beam switching. Turk J Elec Eng & Comp Sci 2017; 25: 539-551.

[8] Encinar JA, Arrebola M, de la Fuente LF, Toso G. A transmit–receive reflectarray antenna for direct broadcast satellite applications. IEEE T Antennas Propag 2011; 9: 3255-3264.

[9] Encinar JA, Datashvili L, Zornoza JA, Arrebola M, Sierra–Castaner M, Besada JL, Baier H, Legay H. Dual–polarization dual–coverage reflectarray for space applications. IEEE T Antennas Propag 2006; 10: 2827–2837.

[10] Han C, Zhang Y, Yang Q. A novel single-layer unit structure for broadband reflectarray antenna. IEEE Antennas and Wireless Propagation Letters 2017; 16: 681-684.

[11] Genc A, Basyigit IB, Colak B, Helhel S. Investigation of the characteristics of low-cost and lightweight horn array antennas with novel monolithic waveguide feeding networks. AEU-International Journal of Electronics and Communications 2018; 89: 15-23.

[12] Deng R , Xu S, Yang F, Li M. Design of a low-cost single-layer X/Ku dual-band metal-only reflectarray antenna. IEEE Antennas and Wireless Propagation Letters 2017; 16: 2106-2109.

[13] Fuentes JAO, Montero JS, Lopez JIM, Cuevas JR, Martynyuk AE. Dual-frequency reflectarray based on split-ring slots. IEEE Antennas and Wireless Propagation Letters 2016; 16: 952-955.

[14] Florencio R, Encinar JA, Boix RR, Losada V, Toso G. Reflectarray antennas for dual polarization and broadband telecom satellite applications. IEEE T Antennas Propag 2015; 4: 1234-1246.

[15] Wang Q, Shao ZH, Cheng YJ, Li PK. Ka/W Dual-band reflectarray antenna for dual linear polarization. IEEE Antennas and Wireless Propagation Letters 2016; 16: 1301-1304.

[16] Florencio R, Encinar JA, Boix RR, Pérez G. Palomino. Dual-polarization reflectarray made of cells with two orthogonal sets of parallel dipoles for bandwidth and cross-polarization improvement. IET Microwave Antennas Propag 2014; 15: 1389-1397.

[17] Chaharmir MR, Shaker J, Gagnon N. Broadband dual-band linear orthogonal polarisation reflectarray. Electron Lett 2009; 45: 13-14.

[18] Bialkowski ME. Bandwidth considerations for a microstrip reflectarray. PIER J 2008; 3: 173–187.

[19] Chaharmir MR, Shaker J, Legay H. Broadband design of a single layer large reflectarray using multi cross loop elements. IEEE T Antennas Propag 2009; 10: 3363-3366.

[20] Huang J, Encinar JA. Reflectarray Antennas. Piscataway, NJ, USA: IEEE Press, 2008.